AGU PUBLICATIONS

JGR

Journal of Geophysical Research: Atmospheres

RESEARCH ARTICLE
10.1002/2016JD025510

Key Points:
- MISR-simulated cloud top heights are derived from CloudSat/CALIPSO-retrieved visible extinction profiles and compared with MISR retrievals
- MISR-simulated cloud top heights are in good agreement with MISR retrievals, and middle- and high-topped clouds agree to within 5% cloud area
- Large uncertainties remain in low-topped and total cloud area due to differences in detection of subpixel-scale clouds

Correspondence to:
B. R. Hillman,
bhillma@sandia.gov

Citation:
Hillman, B. R., R. T. Marchand, T. P. Ackerman, G. G. Mace, and S. Benson (2017), Assessing the accuracy of MISR and MISR-simulated cloud top heights using CloudSat- and CALIPSO-retrieved hydrometeor profiles, *J. Geophys. Res. Atmos.*, *122*, 2878–2897, doi:10.1002/2016JD025510.

Received 13 JUN 2016
Accepted 17 FEB 2017
Accepted article online 20 FEB 2017
Published online 7 MAR 2017

Assessing the accuracy of MISR and MISR-simulated cloud top heights using CloudSat- and CALIPSO-retrieved hydrometeor profiles

Benjamin R. Hillman[1], Roger T. Marchand[2], Thomas P. Ackerman[2,3], Gerald G. Mace[4], and Sally Benson[4]

[1]Sandia National Laboratories, Albuquerque, New Mexico, USA, [2]Department of Atmospheric Sciences, University of Washington, Seattle, Washington, USA, [3]Joint Institute for the Study of the Atmosphere and Ocean, University of Washington, Seattle, Washington, USA, [4]Atmospheric Sciences, University of Utah, Salt Lake City, Utah, USA

Abstract Satellite retrievals of cloud properties are often used in the evaluation of global climate models, and in recent years satellite instrument simulators have been used to account for known retrieval biases in order to make more consistent comparisons between models and retrievals. Many of these simulators have seen little critical evaluation. Here we evaluate the Multiangle Imaging Spectroradiometer (MISR) simulator by using visible extinction profiles retrieved from a combination of CloudSat, CALIPSO, MODIS, and AMSR-E observations as inputs to the MISR simulator and comparing cloud top height statistics from the MISR simulator with those retrieved by MISR. Overall, we find that the occurrence of middle- and high-altitude topped clouds agrees well between MISR retrievals and the MISR-simulated output, with distributions of middle- and high-topped cloud cover typically agreeing to better than 5% in both zonal and regional averages. However, there are significant differences in the occurrence of low-topped clouds between MISR retrievals and MISR-simulated output that are due to differences in the detection of low-level clouds between MISR and the combined retrievals used to drive the MISR simulator, rather than due to errors in the MISR simulator cloud top height adjustment. This difference highlights the importance of sensor resolution and boundary layer cloud spatial structure in determining low-altitude cloud cover. The MISR-simulated and MISR-retrieved cloud optical depth also show systematic differences, which are also likely due in part to cloud spatial structure.

1. Introduction

Clouds are critically important to the Earth climate system, and cloud feedback processes are a primary source of uncertainty in projections of future climate [*Cess et al.*, 1990; *Bony and Dufresne*, 2005; *Williams and Webb*, 2009; *Medeiros et al.*, 2008; *Dufresne and Bony*, 2008; *Bony et al.*, 2006]. This makes evaluation of cloud properties in large-scale models of utmost importance. Observational records of cloud occurrence and other properties from satellite imager retrievals including the International Satellite Cloud Climatology Project (ISCCP) [*Rossow and Schiffer*, 1999], the Moderate Resolution Imaging Spectroradiometer (MODIS) [*King et al.*, 2003], and the Multiangle Imaging Spectroradiometer (MISR) [*Diner et al.*, 2002, 2005] provide an attractive baseline for model evaluation, because they provide near-global coverage and an increasingly long time series. But comparisons between satellite imager retrievals of cloud properties and modeled clouds are difficult because of limitations in the way clouds and their properties are identified and retrieved by satellites. In particular, cloud top height or cloud top pressure retrievals based on visible or infrared observations are known to have significant problems when clouds with low amounts of condensate (i.e., nonopaque clouds or cloud tops) are present, especially multilayer clouds where the upper layer cloud is optically thin [*Marchand et al.*, 2010; *Pincus et al.*, 2012]. Fundamentally, the visible and infrared observations gathered by MODIS, MISR, and ISSCP cannot fully constrain the vertical distribution of condensate, including discriminating between condensate types in differing layers, and this leads to uncertainties and errors in the determination (that is the retrieval) of cloud top height. Models, however, specify (or perhaps one should say resolve) the vertical distribution of condensate to some degree. One can therefore account for errors in the satellite retrieval process by "simulating" the cloud top height or cloud top pressure a satellite would observe given the model cloud field and obtain a better evaluation of the model cloud top by comparing the satellite simulated cloud top height with the satellite retrieval, rather than comparing the true cloud top height from the model with the satellite retrieval.

For example, in the case of infrared (IR) imager retrievals of cloud top height such as those from ISCCP, the quantity retrieved does not directly identify the true cloud top height, but rather a radiative effective cloud top height that is inferred from the IR brightness temperature and a temperature profile. The ISCCP simulator introduced by *Klein and Jakob* [1999] has been widely used in model comparisons with ISCCP observations to account for the difference [*Webb et al.*, 2001; *Norris and Weaver*, 2001; *Lin and Zhang*, 2004; *Zhang et al.*, 2005; *Wyant et al.*, 2006; *Klein et al.*, 2013]. The ISCCP simulator produces joint histograms of cloud top pressure and cloud optical depth from model fields that can be directly compared with joint histograms produced by ISCCP. In effect, each bin in the ISCCP histogram (sometimes referred to as a cloud type or cloud component) is a cloud fraction that quantifies how often clouds within a certain range of cloud top pressures and cloud optical depths occur, and with the sum of all bins yielding the total cloud cover. Because outgoing longwave radiation is strongly influenced by cloud top height and outgoing shortwave radiation is strongly influenced by cloud optical depth, comparisons using the ISCCP joint histograms provide an evaluation of model cloud amount that is linked to the impact of clouds on the model radiation budget. The utility of the ISCCP simulator has inspired efforts to construct simulators for additional satellite cloud-observing platforms, including MISR [*Marchand and Ackerman*, 2010] and MODIS [*Pincus et al.*, 2012]. The MISR and MODIS simulators are likewise now being used in comparisons between models and observations, nominally leading to more robust evaluation of model clouds [e.g., *Kay et al.*, 2012].

While the goal of the instrument simulator approach is to remove ambiguities in comparisons between models and observations such that remaining differences between the observed and simulated cloud properties can be interpreted as model errors, the simulators themselves have seen little critical evaluation. *Mace et al.* [2011], hereafter M2011, performed an evaluation of the ISCCP simulator using thermodynamic and cloud property profiles derived from data collected at the Atmospheric Radiation Measurement Program (ARM) [*Ackerman and Stokes*, 2003] Southern Great Plains (SGP) ground-based observing site located near Lamont, Oklahoma. In their analysis, M2011 compare ARM radar- and lidar-derived cloud properties directly to those retrieved from ISCCP to first assess the biases in the ISCCP retrieval relative to the ARM-derived cloud properties. They then apply the ISCCP simulator to the ARM-derived profiles of cloud extinction and compare the ISCCP-simulated cloud properties to ISCCP retrievals. They find that the simulator accounts for much of the bias in the ISCCP cloud top pressure (p_c) retrieval; that is, the ISCCP-simulated p_c retrieval compares well with the actual ISCCP retrieval. However, midlevel cloud remained a problem with significantly less midlevel cloud in the simulated retrievals than in the ISCCP retrievals (6% relative to the total number of profiles, or equivalently, 23% relative to the amount of simulated midlevel cloud), suggesting that the simulator does not completely compensate for the well-known tendency of ISCCP retrievals to overestimate the amount of midlevel clouds [e.g., *Marchand et al.*, 2010]. Perhaps more problematically, M2011 found large differences in optical depth between ISCCP and ARM retrievals. M2011 suggest this may be due to a combination of subpixel variability in the clouds and limitations associated with the 1-D radiative transfer used in the ISCCP retrievals. We will discuss this topic in more detail later in this article, as it also affects the evaluation of the MISR simulator presented here.

The goal of this study is to perform a similar analysis to M2011 for the MISR simulator. Conceptually similar to the ISCCP simulator, the MISR simulator produces histograms of cloud optical depth and cloud top height. While the optical depth retrievals are similar between ISCCP and MISR, the MISR cloud top height is based on a geometric stereo-imaging technique that has different strengths and weaknesses relative to ISCCP. MISR provides more accurate retrievals of cloud top height for low-level and midlevel clouds, more reliable discrimination of midlevel clouds from other clouds, and is insensitive to instrument calibration making the data well suited for examining variability on seasonal or longer time scales, while ISCCP provides a longer time record, diurnal sampling, and is able to better detect optically thin high-level clouds because of its use of thermal IR observations.

Section 2 describes the analysis approach and data sets, while comparisons between MISR-simulated cloud top height and MISR retrievals are shown in section 3. Section 4 discusses the effect that sampling at different times of the day might have on the results in section 3, and a summary of our findings and additional discussion is presented in section 5.

2. Data and Methods

Following the analysis approach used by M2011 for the ISCCP simulator, we evaluate the MISR simulator by driving the MISR simulator with profiles of visible extinction derived using a combination of radar and

lidar retrievals. Cloud top height and optical depth joint histograms diagnosed by the MISR simulator are aggregated for selected regions and time periods and compared with similarly aggregated MISR retrievals. These two data sets are compared in order to assess how well the MISR simulator is able to reproduce MISR observations given the nominally "true" radar-lidar vertical profiles of cloud occurrence and extinction. We note that the CloudSat and CALIPSO satellites orbit in the A-train constellation, along with the Aqua satellite that includes a MODIS instrument. These satellites, flying in close formation, allow for nearly coincident observations that promote data fusion products like the visible extinction retrieval used here. The MISR instrument, on the other hand, flies on the Terra satellite, which has an equatorial crossing time about 3 h earlier. Therefore, the different diurnal sampling times of the satellites are expected to affect our comparison of MISR and MISR-simulated retrievals to some extent. We expect these diurnally driven differences to be small in most regions (see section 4).

The MISR cloud top height and optical depth (CTH-OD) data used here is the Version 6 product [*Marchand et al.*, 2010], which is produced at the NASA Langley Distributed Active Archive Centers. MISR V6 Monthly CTH-OD data are available via the Earth System Grid (https://pcmdi.llnl.gov/search/esgf-llnl/) under the obs4mips project (variable clMISR), as well as the Cloud Feedback Model Intercomparison Project (CFMIP) (http://cfmip.metoffice.com/) data archive being hosted at IPSL (http://climserv.ipsl.polytechnique.fr/cfmip-obs/). In this manuscript orbit level (rather than monthly aggregated) data were used in order to estimate sampling uncertainties. Presently, the orbit level data are not publicly visible but may be obtained by special request to the authors of this manuscript or the Jet Propulsion Laboratory MISR project. The only difference between the previous version (V5) of the CTH-OD data set (described in *Marchand et al.* [2010]) and the V6 used here is improved sea ice masking that removed some problematic data at high latitudes. A version 7 (V7) of the MISR CTH-OD product is in development, will be based on an improved version of the MISR CTH retrieval, and will be documented in future publications.

The MISR instrument consists of nine "push-broom" cameras pointed at nine different view angles. Each camera images in four spectral bands (443, 555, 670, and 865 nm) with a resolution of approximately 275 m and a swath width of 400 km. Cloud top height and optical depth retrievals are performed at an effective resolution (or "pixel size") of approximately 1.1 km. The different view angles from the MISR cameras enable the use of a stereoscopic technique for the retrieval of cloud top heights [*Moroney et al.*, 2002; *Muller et al.*, 2002]. The advantage of the MISR retrieval of cloud top height (over radiometric retrievals based on IR brightness temperature) is that the retrieved cloud top heights are not sensitive to the radiometric calibration, and cloud top heights are retrieved with little bias when cloud is detected [*Marchand et al.*, 2007; *Naud et al.*, 2002, 2004, 2005; *Seiz et al.*, 2006; *Marchand et al.*, 2001]. Larger discrepancies in retrieved heights can arise when MISR encounters optically thin cloud layers, which may be missed by the MISR pattern matcher. It is primarily these cases which the MISR simulator is designed to account for (described below in the context of Figure 2). Cloud optical depth is retrieved for cloudy pixels from the observed visible radiance at 865 nm assuming a one-dimensional single-layer cloud with a fixed effective radius and no aerosol. The retrieval uses radiances from the MISR camera closest to nadir with no Sun glint. More details on the MISR cloud top height and optical depth retrievals as well as a discussion of features and uncertainties in the retrievals as compared with ISCCP and MODIS can be found in *Marchand et al.* [2010, and references therein]. MISR optical depth retrievals are performed over open ocean but not over land or ice surfaces, which makes direct comparison between ARM ground-based retrievals and coincident MISR cloud top height and optical depth (CTH-OD) retrievals impossible; therefore, we cannot compare MISR data with ARM data as done by M2011.

Our approach is to test the MISR simulator using profiles of cloud visible extinction derived using data and retrievals from CloudSat, CALIPSO, MODIS, and AMSR-E. The retrieval approach is essentially that used in *Mace and Wrenn* [2013] and *Berry and Mace* [2014] with ice cloud microphysical properties taken from the CloudSat 2C-ICE product [*Deng et al.*, 2010, 2013] following *Berry and Mace* [2014]. Thermodynamic profiles are based on European Centre for Medium-Range Weather Forecasts (ECMWF) data mapped to the CloudSat track in the CloudSat auxiliary product known as ECMWF-AUX. Column visible optical depths from the CloudSat cloud optical depth product (2B-TAU, which uses MODIS radiances) are used. With the exception of the use of 2C-ICE, the most detailed description of this technique can be found in *Mace* [2010]. Specifically, the hydrometeor layer occurrences from combined CloudSat radar and CALIPSO lidar data from the Radar-Lidar Geometrical Profile Product (RL-GEOPROF) [*Mace et al.*, 2009; *Mace and Zhang*, 2014] Version R04 define the vertical hydrometeor occurrence distribution. In RL-GEOPROF, CALIPSO lidar detections are mapped onto the coarser CloudSat grid (with an along-track horizontal resolution of approximately 2 km, a horizontal grid spacing of

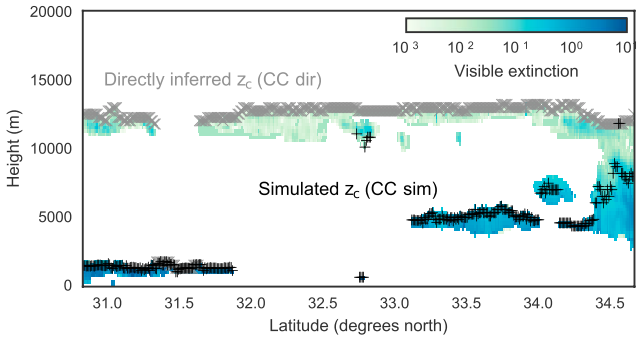

Figure 1. Visible extinction profiles derived from CloudSat cloud profiling radar and CALIPSO cloud lidar for a short orbit segment. Cloud top height for each profile estimated directly by taking the highest altitude with nonzero extinction (CC-dir) is indicated with grey "cross" markers, and cloud top height estimated using the MISR simulator (CC-sim) is indicated with black "plus" markers.

about 1 km and vertical grid spacing of 240 m). Only radar volumes that are at least 50% filled by lidar detections are treated as having a cloud detection on the CloudSat/retrieval grid. This threshold has a notable effect on the resulting low-cloud fractions (see Figure 5 and discussion in section 3). The properties of warm liquid phase clouds are derived by combining CloudSat radar reflectivity factors with optical depths from the CloudSat 2B-TAU product and liquid water paths from AMSR-E applying essentially the *Dong and Mace* [2003] retrieval [see *Mace*, 2010, Appendix A]. For radar volumes where condensate is only detected by the lidar, a radar reflectivity value below the sensitivity of CloudSat (−35 dBZe) is assumed; a default liquid water path of 200 g/m^2 is used in instances where neither optical depth nor liquid water path retrievals are successful. For radar volumes with temperatures colder than the freezing level, an estimate is made of the liquid water path fraction that is above the freezing level to temperatures as low as 240 K as described in *Mace et al.* [2006] and is added to the 2C-ICE extinction.

The MISR simulator provides estimates of the cloud top height (z_c) that MISR would likely retrieve (from a given input profile of visible extinction) based on a number of simple rules, described in detail in *Marchand and Ackerman* [2010], which we briefly summarize in the context of Figure 1. The colors in Figure 1 show an example of the combined CloudSat and CALIPSO (hereafter referred to as CC) cloud visible extinction retrieval for a short orbit section. The cloud top height estimated using two different methods is overlaid on the panel. First, cloud top height is estimated directly as the highest altitude bin (based on the MISR cloud top height grid) for which the visible CC extinction is nonzero. This direct estimate of cloud top height (hereafter referred to as CC-dir) is indicated on the figure for each profile with a grey "cross," with the vertical position of the "cross" denoting the location of the altitude bin midpoint. Next, the simulated cloud top height (hereafter referred to as CC-sim) is diagnosed by passing the profiles of visible extinction to the MISR simulator, indicated in the figure for each profile with a black "plus" symbol. This example highlights several key aspects of how the MISR simulator works. For single-layer water clouds, the MISR estimate of cloud top height is expected to be in good agreement with the "true" cloud top height. For example, the extinction profile near 31.5°N shows a single low-level cloud layer with large optical depth, and both the CC-dir and CC-sim estimates of cloud top height agree. For multilayer profiles where the upper cloud layer is sufficiently thin (nominally $\tau < 1$), MISR retrievals tend to see through the upper level cloud and retrieve the cloud top height of the lower cloud layer. The MISR simulator mimics this tendency and so CC-sim returns the cloud top height of the lower cloud layer in this case. An example of this situation is seen in Figure 1 near 33.5°N. The threshold value of $\tau < 1$ to identify layers that the MISR stereo retrieval would likely miss is based on an analysis by *Marchand et al.* [2007] comparing MISR stereo height retrievals with height and visible extinction retrievals derived from a combination of ARM ground-based radar and lidar. For clouds with optically thicker ice-phase tops, the MISR simulator penetrates down into the cloud layer to retrieve the cloud top height where the integrated optical depth reaches a nominal value of $\tau = 1$ (again following analysis by *Marchand et al.* [2007]). In these cases (such as near 34.5°N in Figure 1), the simulated (CC-sim) cloud top height will also be lower than that calculated directly by taking the highest level with nonzero extinction (CC-dir). The sensitivity of the results presented here to the $\tau > 1$ threshold for identifying optically opaque layers will be explored later in the manuscript in the context of Figure 7.

Figure 2 shows joint histograms of cloud top height and cloud optical depth (the vertical sum of the nondimensionalized visible extinction represented by the shading in Figure 1) for the example orbit segment shown in Figure 1 using both the CC-sim and CC-dir methods of estimating cloud top height described above. The MISR simulator does not currently include any corrections to the input visible extinction to account for limitations in the MISR retrieval of cloud optical depth (such as assumed particle size or 3-D effects). Thus, the

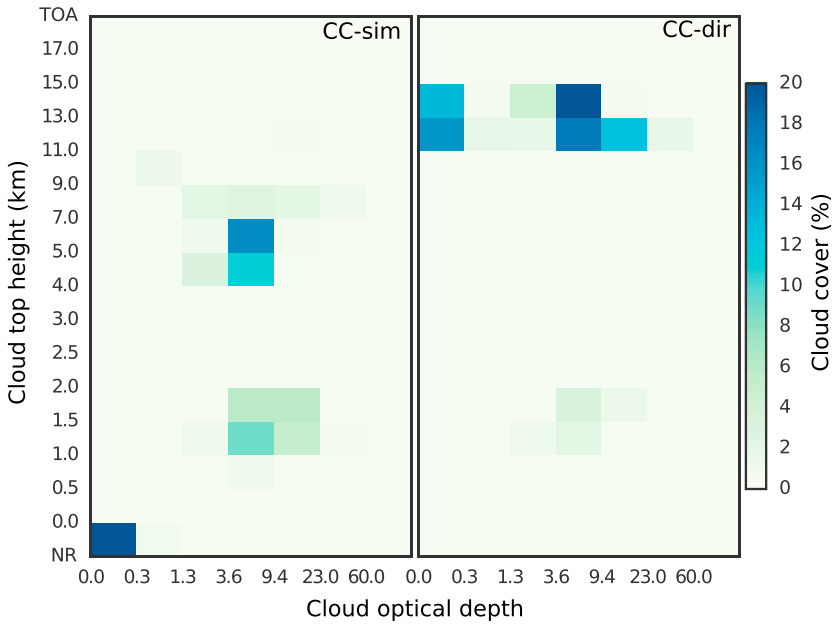

Figure 2. Joint histograms of cloud top height and optical depth for the example orbit segment shown in Figure 1. (left) Joint histograms created using cloud top heights diagnosed using the MISR simulator (CC-sim) and (right) joint histograms created using cloud top heights diagnosed by taking the highest altitude with nonzero extinction (CC-dir).

integrated column optical depths from CC-sim and CC-dir for a given column (pixel) are identical. The value of each element in the joint histogram is the relative frequency of occurrence of profiles within a certain cloud top height and optical depth range, and because each profile is assigned only one value of cloud top height and one value of cloud optical depth, the sum of the joint histogram values over all bins is equal to the total vertically projected cloud cover. We can likewise take the sum over all bins with cloud top height $0 \le z_c < 3$ km to obtain the low-topped cloud cover, the sum over all bins with cloud top height $3 \le z_c < 7$ km to obtain the mid-topped cloud cover, and the sum over all bins with cloud top height $z_c \ge 7$ km to obtain the high-topped cloud cover. Taking the sum across the columns of the joint histogram yields the marginal histogram of cloud top height, and taking the sum across the rows yields the marginal histogram of cloud optical depth. Because the MISR retrieval has difficulty detecting clouds with optical depths $\tau < 0.3$, we generally opt to take these sums over only those bins with $\tau > 0.3$. Because the MISR simulator does *not* correct for any biases in the retrieval of cloud optical depth, the marginal histograms of cloud optical depth (the sum over all cloud top height bins) are identical between the CC-sim and CC-dir data sets.

The CC-sim joint histogram (Figure 2) for this orbit has one low-topped mode with $0.5 \le z_c < 2.0$ km (corresponding primarily to the low-level cloud at the far left of the top part of Figure 1) and a mid-topped mode with $4.0 \le z_c < 9.0$ km (corresponding to the midlevel and deep cloud layers at the right of the top part of the figure). There is also a large amount of cloud in the CC-sim joint histogram with $z_c < 0$ km. This cloud top height bin (referred to as the "no retrieval" bin and labeled "NR" in the figure) is reserved for profiles for which the MISR simulator determines that MISR would fail to retrieve a cloud top height. This often occurs for columns with very low optical depths. These no-retrieval cases correspond to the section of the example orbit in Figure 1 with a single-layer thin high-level cloud, between 32 and 33°N, for which no simulated height retrieval is shown on the figure. The CC-dir joint histogram is dominated by a high-topped mode with $11.0 \le z_c < 15.0$ km. There is also a less prominent low-topped mode with $1.0 \le z_c < 2.0$ km, corresponding to the short section of the orbit with single-layered low-level cloud around 31.5°N.

The following section presents comparisons for two separate months (January and June 2008) of aggregated MISR, CC-sim, and CC-dir retrievals. The orbit level retrievals of cloud top height and cloud optical depth joint histogram counts from MISR, CC-sim, and CC-dir are aggregated onto a common 5° by 5° latitude-longitude grid. This relatively coarse-resolution grid is needed to obtain sufficient sampling for the comparisons with the relatively short time span evaluated and the limited spatial sampling of CloudSat and CALIPSO, both of which

Table 1. Regional Mean Cloud Cover by Cloud Top Height for January 2008 from MISR Retrievals and From MISR-Simulated Retrievals Performed on CloudSat/CALIPSO Extinction Profiles (CC-Sim)[a]

Region	Type	MISR	CC-Sim	Diff	*p* Value	Significance
Pacific	High	13.7	13.5	−0.2	0.234	
	Mid	13.7	14.8	1.1	0.017	*
	Low	43.4	35.0	−8.4	0.000	**
	Total	72.8	64.3	−8.4	0.000	**
N. Pacific	High	23.0	8.1	−14.9	0.000	**
	Mid	17.2	26.8	9.6	0.000	**
	Low	38.3	49.5	11.2	0.010	**
	Total	81.8	85.3	3.4	0.513	
Tropical W. P.	High	30.8	35.7	4.9	0.238	
	Mid	12.7	12.3	−0.4	0.771	
	Low	31.0	18.4	−12.7	0.000	**
	Total	75.5	68.8	−6.8	0.021	*
California S. C.	High	20.3	15.6	−4.7	0.958	
	Mid	5.4	9.4	4.0	0.056	
	Low	43.9	43.9	0.0	0.833	
	Total	73.1	70.2	−2.9	0.572	
Hawaiian T. C.	High	14.2	8.4	−5.8	0.015	*
	Mid	8.5	8.3	−0.1	0.739	
	Low	36.7	36.1	−0.6	0.955	
	Total	60.1	53.7	−6.4	0.016	*
S. Pacific	High	9.2	13.3	4.1	0.011	*
	Mid	19.0	17.9	−1.1	0.132	
	Low	50.0	41.0	−9.0	0.004	**
	Total	80.8	73.1	−7.7	0.000	**

[a]Also shown are the differences (CC-sim minus MISR) and the significance of the differences calculated using the Student's *t* test on the orbit level means.
*Statistical significance at the 95% confidence level.
**Statistical significance at the 99% confidence level.

perform retrievals over a linear transect as opposed to the 400 km swath that MISR samples. Because comparisons are done in a statistical sense on the aggregated retrievals, care must be taken to account for sampling uncertainties. Where appropriate, we calculate 95% confidence intervals for derived statistics (such as the monthly mean total cloud cover) using a bootstrap resampling technique [*Efron and Tibshirani*, 1994; *Wilks*, 2011] or in the case of Tables 1 and 2, using a Student *t*-test (and making the conservative assumption that each MISR orbit represents a single independent sample).

Because the MISR simulator does not attempt to correct for any inherent biases in the MISR retrieval of cloud optical depth, the primary goal of the remainder of the manuscript is to assess the performance of the simulator in correcting for MISR cloud top height retrieval biases. However, differences in the retrieval of cloud optical depth between MISR and CC provide insights into the source of differences in cloud top height statistics, and so analysis of differences in the cloud optical depth domain is included as well.

3. Comparison of MISR and MISR-Simulated Retrievals

3.1. Cloud Cover by Cloud Top Height

Figures 3 and 4 show low-topped, mid-topped, high-topped, and total cloud cover from MISR retrievals and diagnosed from the CC visible extinction profiles with and without using the MISR simulator (CC-sim and CC-dir, respectively) for the months of January and June 2008. Data are bounded by −70°N to 70°N latitude and 100°E to −70°E longitude (this includes ocean surfaces beyond the Pacific Ocean, but we will refer to this domain as "Pacific" for convenience). Boxes are drawn around five climatically distinct regions that we will

Table 2. As in Table 1 but for June 2008[a]

Region	Type	MISR	CC-Sim	Diff	*p* Value	Significance
Pacific	High	15.6	16.1	0.6	0.114	
	Mid	11.1	33.2	−7.0	0.000	**
	Total	69.4	63.7	−5.7	0.003	**
N. Pacific	High	10.1	15.8	5.7	0.009	**
	Mid	19.0	24.1	5.2	0.003	**
	Low	61.2	47.3	−13.9	0.000	**
	Total	94.2	87.8	−6.5	0.001	**
Tropical W. P.	High	31.9	31.7	−0.2	0.546	
	Mid	11.8	16.2	4.4	0.043	*
	Low	24.1	17.3	−6.8	0.008	**
	Total	68.2	66.8	−1.5	0.547	
California S. C.	High	1.7	1.5	−0.2	0.504	
	Mid	2.0	2.9	0.9	0.358	
	Low	65.4	52.7	−12.8	0.050	
	Total	76.0	57.5	−18.5	0.005	**
Hawaiian T. C.	High	9.7	11.7	2.0	0.891	
	Mid	5.3	5.1	−0.2	0.824	
	Low	42.0	31.2	−10.8	0.000	**
	Total	61.4	49.4	−12.1	0.000	**
S. Pacific	High	17.2	12.4	−4.8	0.045	*
	Mid	14.6	15.4	0.8	0.819	
	Low	42.9	53.1	10.2	0.000	**
	Total	78.7	81.6	2.9	0.021	*

[a]Also shown are the differences (CC-sim minus MISR) and the significance of the differences calculated using the Student's *t* test on the orbit level means.
*Statistical significance at the 95% confidence level.
**Statistical significance at the 99% confidence level.

investigate more closely: the North Pacific (35°N to 60°N; 160°E to −140°E), Hawaiian Trade Cumulus (15°N to 35°N; 160°E to −140°E), California Stratocumulus (15°N to 35°N; −140°E to −110°E), Tropical Western Pacific (−5°N to 20°N; 70°E to 150°E), and the South Pacific (−60°N to −30°N; −180°E to −80°E).

The MISR simulator results (CC-sim; Figures 3 and 4, second columns) are broadly similar to the MISR observations (Figures 3 and 4, first columns), particularly when compared with CC-dir. This indicates that (at least qualitatively) the MISR simulator is working as intended. Differences between CC-dir and CC-sim (and likewise between CC-dir and MISR) are especially large in the Tropical Warm Pool, North Pacific, and South Pacific regions, owing to the large occurrence of optically thin high-altitude cloud in these regions. Averaged over the entire region shown in the figure, the occurrence of high-topped clouds differs by only 2% cloud cover in January and June 2008 between CC-sim and MISR, and the occurrence of mid-topped clouds differs by only 2% cloud cover in January, and by 3% in June. These differences are small, but some amount of cancelation of errors due to averaging over such a large area is likely partly responsible for such good agreement. This is explored later in the context of Tables 1 and 2, in which it is shown that differences in high-topped and mid-topped clouds are still typically less than 5% cloud area. The largest difference between MISR and CC-sim is in low-topped cloud, where the low-topped cloud cover is smaller in CC-sim by 9% in January and 7% in June. However, much of this difference appears to be due to differences in low-level cloud detection between MISR and CC, rather than due to errors in the MISR simulator determination of cloud top height. This is supported by the estimates of total cloud cover, which differ by 8% and 6% in January and June, respectively. This difference is primarily due to clouds which are identified by MISR as being optically thin and having cloud tops at low altitudes.

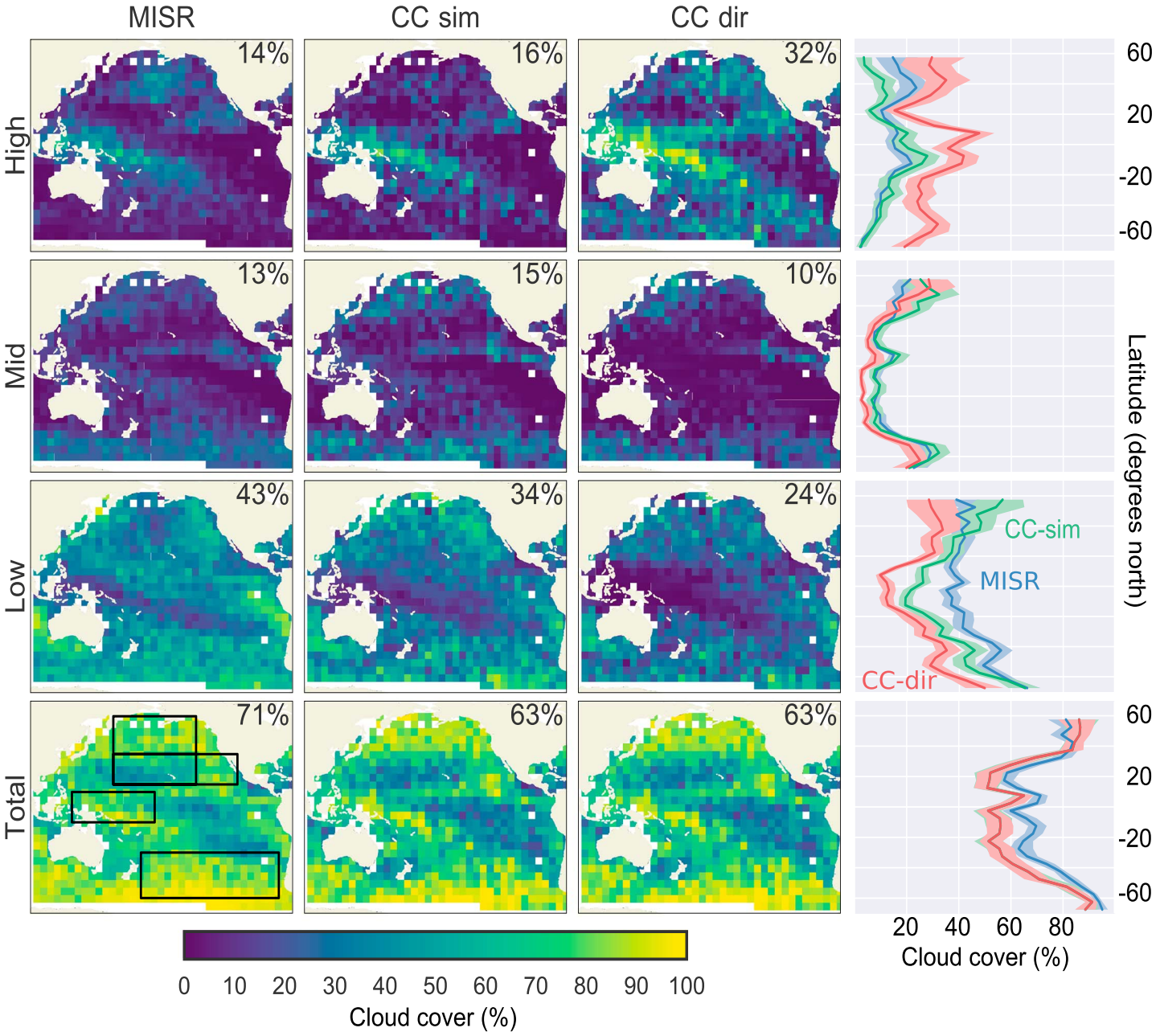

Figure 3. From top to bottom, (first row) High-topped ($z_c \geq 7$ km), (second row) mid-topped ($3 \leq z_c < 7$ km), (third row) low-topped ($0 \leq z_c < 3$ km), and (fourth row) total cloud cover from (first column) MISR, (second column) CC-sim, and (third column) CC-dir for the month of January 2008. Area-weighted means are indicated on each panel. Boxes are drawn around particular study regions (from top to bottom and left to right): North Pacific, Hawaiian Trade Cumulus, California Stratocumulus, Tropical Western Pacific, and the South Pacific. Zonally averaged cloud cover for each cloud type is shown in Figure 3 (fourth column). Shaded regions indicate 95% confidence intervals obtained using 1000 bootstrap resamples of orbit level zonal means. Orbit level data have been aggregated onto a 5° latitude-longitude grid.

The large impact that the MISR simulator has on estimated cloud top height is perhaps clearer in the zonal average, which is shown in Figures 3 and 4 (fourth columns). Shaded regions show the 95% confidence interval, based on 1000 bootstrap resamples of the orbit level zonal means. A large fraction of the high-topped cloud detected by CALIPSO is not identified by the MISR stereo height retrieval, largely because it is optically thin. The MISR-simulated high-topped cloud cover is generally in good agreement with the MISR retrievals, except perhaps at northern midlatitudes in January (30°–60°N) and at high southern latitudes in June (south of 50°S) where differences are closer to 10%. This may be due to either MISR detecting thinner

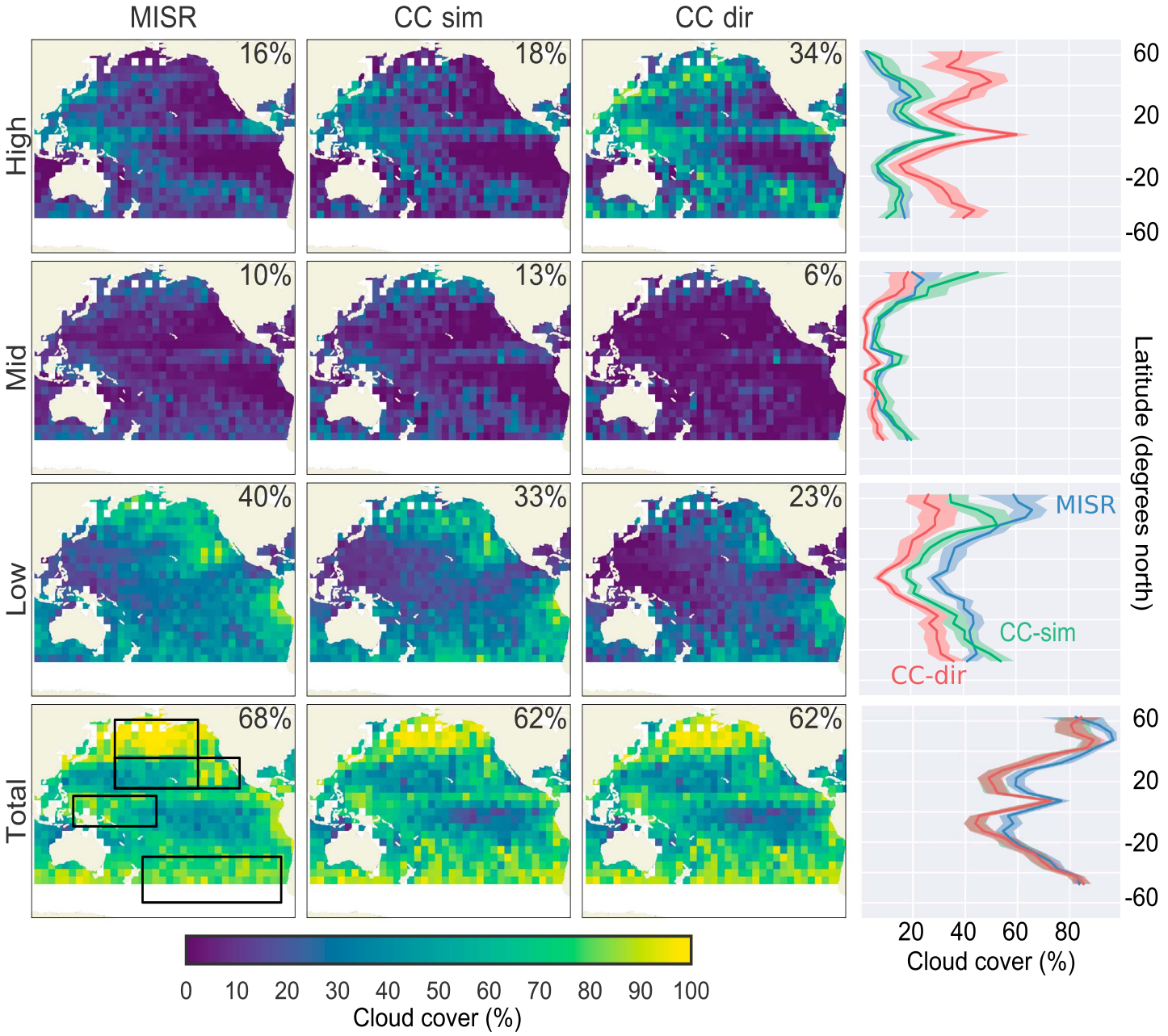

Figure 4. As in Figure 3 but for June 2008.

cirrus in these regions (i.e., clouds with an optical depth $\tau < 1$) because of contrast generated from long solar slant paths through the cirrus or limitations in the MISR stereo height algorithm. When cloud wind speed is successfully retrieved by the MISR data processing, the CTH-OD product uses the MISR stereo height retrieval with winds (the so-called "best winds" retrieval); otherwise, it uses the stereo height "without wind" correction. The MISR stereo image matcher is currently being upgraded, and the upgraded code (which will eventually lead to Version 7 of the MISR CTH-OD product) produces many more successful wind retrievals. Preliminary analysis of MISR CTH-OD Version 7 data indicates somewhat lower amounts of high-topped cloud in the North Pacific (closer to the CC-sim results), suggesting that the 10% difference here may be an error due to incomplete wind speed correction.

The mid-topped MISR-simulated cloud cover is also in very good agreement with the MISR retrievals, except perhaps for middle to high northern latitudes (north of 40°N in January and 50°N in June). Uncertainty bars

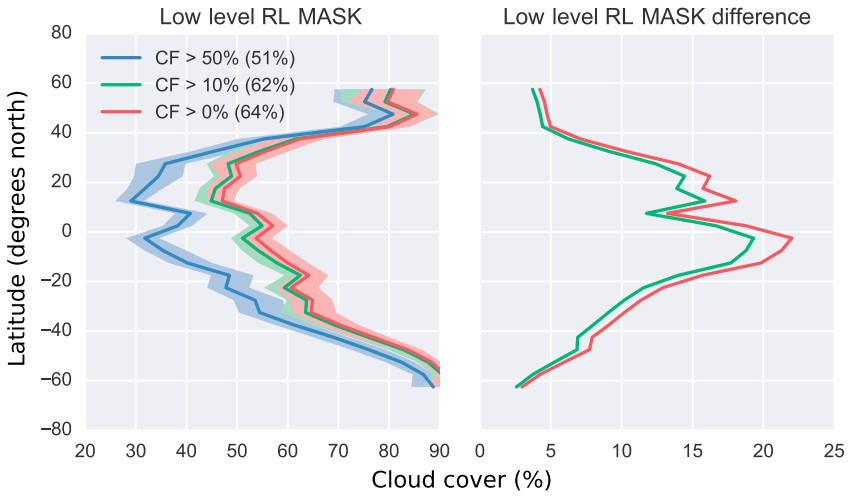

Figure 5. Joint radar-lidar low-level cloud mask from 2B-GEOPROF and 2B-GEOPROF-LIDAR for different lidar cloud fraction thresholds over the Pacific domain. Height bins for each profile are considered "cloudy" if the radar cloud mask (`CPR_Cloud_Mask` in 2B-GEOPROF files) has a value greater than 20 or if the lidar cloud fraction (`CloudFraction` in 2B-GEOPROF-LIDAR files) is greater than the selected threshold value (indicated in the legend). Plotted are the (left) zonally averaged fraction of profiles with any cloudy height bins below 3 km and (right) differences relative to the default threshold of 50%. Numbers in parentheses in the legend indicate the average over the entire (Pacific) domain.

are large at these latitudes, because there is relatively little mid-topped cloud and relatively little ocean area at these latitudes. Nonetheless, it may well be that the MISR simulator is overestimating the amount of MISR mid-topped cloud at these northern latitudes, and we will examine the North Pacific in more detail below.

There are large differences between MISR and CC-sim in the amount of low-topped cloud. The occurrence of MISR low-topped cloud is much larger than CC-sim nearly everywhere except at high northern latitudes in January (north of 40°N) and at high southern latitudes in June (south of about 50°S) where CC-sim total and low-topped cloud exceed MISR. This difference in low (and total cloud) fraction is likely due to differences in the instrument field-of-view or "pixel size." Because the field-of-view or "pixel size" of satellite instruments can be partially filled by clouds, the fraction of satellite pixels containing some amount of cloud (what one might call the retrieved cloud fraction) will be larger than the true fractional area covered by clouds, and this difference generally increases as the satellite pixel size is increased [*Di Girolamo and Davies*, 1997]. Of course, satellite retrievals do not perfectly identify partially cloud-filled pixels as cloudy, and there is a partial cancelation of error that typically results in the satellite-retrieved cloud cover being closer to the true fractional area covered clouds than would be produced by a perfect cloud detector with the same resolution [*Wielicki and Parker*, 1992]. This resolution effect is particularly important for trade cumulus but applies to all broken boundary layer clouds [*Zhao and Di Girolamo*, 2006; *Marchand et al.*, 2010]. The CALIPSO data are mapped onto the coarser CloudSat grid in such a way that a combined retrieval (which uses the CloudSat grid) is only considered to have a lidar detection if 50% of the CloudSat volume is filled by lidar detections; consequently, clouds smaller than 1 km are sometimes missed. This is important because, especially in the trade cumulus regions, clouds smaller than 1 km occur frequently [e.g., *Dey et al.*, 2008]. We have examined the impact of keeping all lidar detections (effectively setting the threshold to 0%) on cloud fraction and found the increase in low-level cloud fraction (all profiles with any cloud below 3 km) to be about 13% in the Pacific mean and as large as 22% in the zonal average in the tropical Pacific (Figure 5). These differences are much smaller at higher latitudes, and differences in the North Pacific are generally less than 5% cloud cover. The resolution-driven increase in MISR-retrieved low-topped cloud due to partially filled pixels is of a similar magnitude [*Jones et al.*, 2012]. The close agreement in total cloud cover between MISR and CloudSat/CALIPSO at high latitudes in the winter hemisphere suggests (or perhaps demonstrates) that low clouds during the winter season at these latitudes are more horizontally continuous (wider). This is especially true in the Southern Hemisphere. Diurnal effects may also contribute to differences between the MISR and CC cloud cover (section 4). Detection of low-topped clouds may also be hindered by surface clutter in CloudSat retrievals, which is known to affect radar returns from the lowest 1 km. This may affect diagnosis of low-topped cloud cover but only for cases

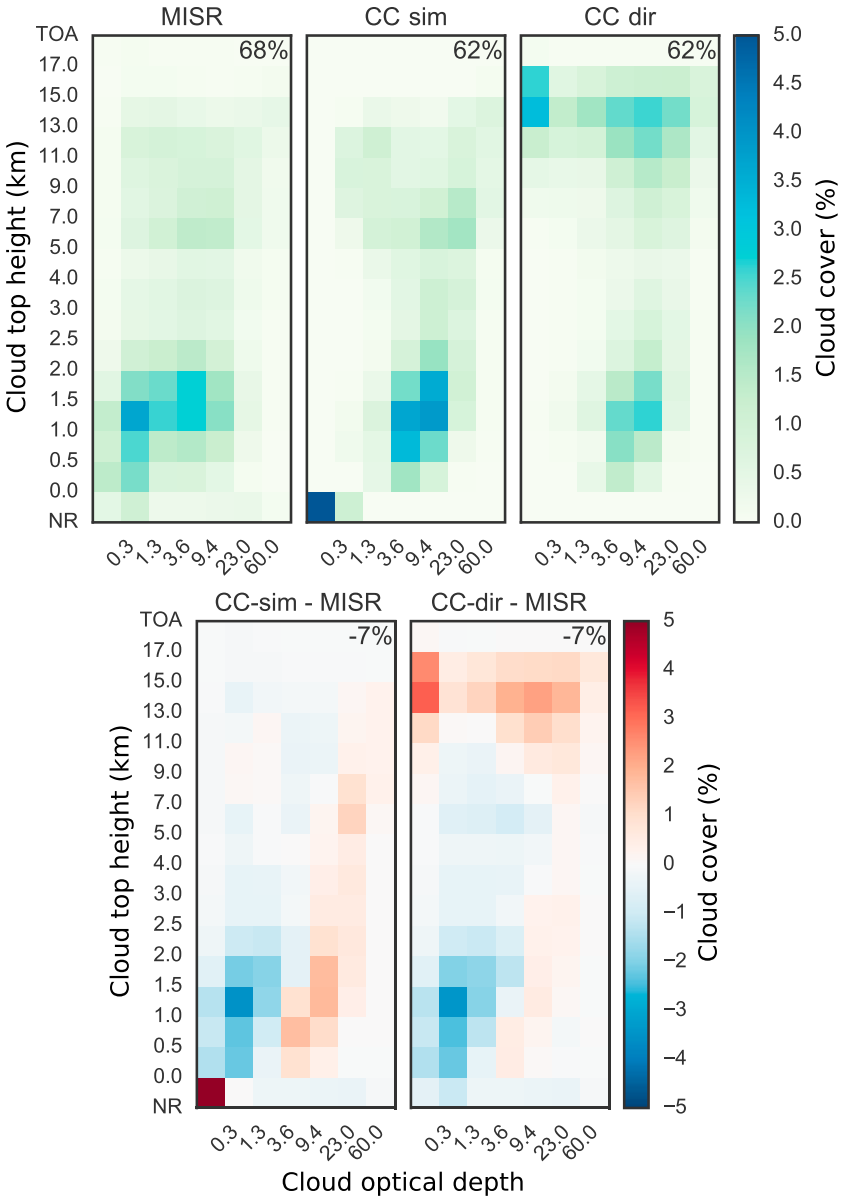

Figure 6. Joint histograms of cloud top height and cloud optical depth aggregated over the Pacific region for the month of June 2008 from (top row) MISR (left), CC-sim (middle), and CC-dir (right), and (bottom row) differences in CC-sim and CC-dir joint histograms relative to MISR (CC-sim minus MISR and CC-dir minus MISR). Numbers in the titles of each panel indicate the total cloud cover (the sum over all bins with optical depth $\tau > 0.3$).

in which the lidar fails to see low clouds due to attenuation by higher-altitude cloud layers. This is unlikely to affect total cloud cover as retrieved by the combination of CloudSat and CALIPSO used here, because the lidar would still detect the presence of cloud somewhere in the column.

3.2. Distributions of Cloud Top Height and Cloud Optical Depth

Full joint histograms for the Pacific region for June 2008 are shown in Figure 6 (top row) and differences between MISR and CC-sim and between MISR and CC-dir are shown in Figure 6 (bottom row) (the joint histograms for the month of January 2008 are remarkably similar and are not shown here). The MISR-retrieved joint histogram has a low-topped ($z_c < 3.0$ km) maximum at low to intermediate optical depths ($\tau < 23$), and a mid-topped to high-topped maximum ($5.0 \leq z_c < 13.0$ km) at intermediate optical depths ($3.6 \leq \tau < 23.0$). The CC-sim joint histogram has a similar bimodal structure, but with considerably smaller amounts of cloud with low optical depth ($\tau < 3.6$) and larger amounts of cloud with large optical depth ($\tau > 23.0$).

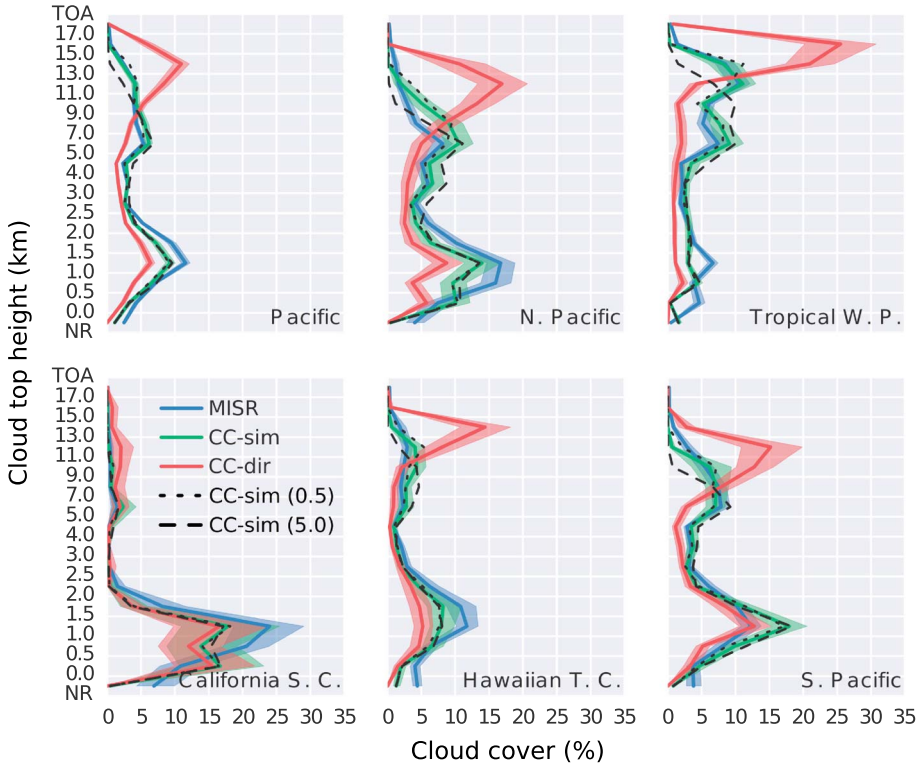

Figure 7. Marginal histograms of cloud top height ($\tau > 0.3$) for each of the regions defined in the text and outlined in Figure 4 for June 2008. Error bars indicate 95% confidence intervals obtained from 1000 bootstrap resamples of orbit level means. Dashed and dotted lines show the sensitivity of simulated cloud top heights to changing the threshold for diagnosing optically opaque layers in the simulator from the default threshold of $\tau > 1.0$ (solid line) to $\tau > 0.5$ (dotted line) and to $\tau > 5.0$. See text for additional discussion.

At first glance, the results shown in Figure 6 can give one the impression that the differences between CC-sim and MISR are larger for low-topped and mid-topped clouds than if one had used CC-dir. But this impression results from two conflating factors: (1) differences in the cloud top height distribution and (2) differences in the optical depth distribution. These factors combine in such a way as to cause the difference in the optical depths to appear to be due to low-topped and mid-topped clouds when using CC-sim and appear to be due to high-topped clouds when using CC-dir.

Recall that the MISR simulator makes no adjustment to the extinction values that are input to the simulator, so CC-sim and CC-dir data sets have exactly the same distributions of column optical depth. CC-sim and CC-dir differ only in the height associated with the retrieved optical depth. As discussed earlier in the context of Figures 1 through 4 (and as will be explored further in the context of Figure 7, below), CC-dir has many more high-altitude cloud tops than CC-sim due to situations where high-altitude cloud with little visible extinction (total optical depth less than about 1 for the high-altitude condensate) occurs above low or midlevel cloud. In this "multilayer" situation, the MISR simulator mimics the tendency of MISR to retrieve the cloud top height of the lower-altitude layer (because the high-altitude layer is optically thin), while the CC-dir diagnosis places the cloud top in the highest-altitude layer with nonzero extinction, even if that extinction is small. But for each pixel, the cloud optical depth associated with the diagnosed cloud top height is the total vertically integrated optical depth, so in the CC-dir case the cloud optical depth of the high-altitude cloud tops appear much larger in the joint histogram than they actually are (due to the contribution from the low-altitude optically thicker clouds). It also often turns out that the total column optical depth from the combined (CC) retrieval is significantly larger than that retrieved from MISR in these cases. As a result of these two conflating factors, the CC-dir joint histogram (Figure 6, top right) shows many more high-topped clouds with an optical depth $\tau > 3.6$ and the CC-sim joint histogram (Figure 6, top middle) shows more mid-topped and low-topped clouds with an optical depth $\tau > 3.6$. The important point here is that the MISR simulator is doing what it is designed

to do: generating a cloud top height from the CC extinction field that is consistent with the MISR cloud top height retrieval.

Differences in optical depth retrievals between passive and active sensors have been noted by other authors. M2011 found a similar optical depth difference in their analysis of ISCCP histograms (finding the ARM radar-lidar data often yield larger optical depths than are retrieved by ISCCP) and suggested that this was likely due to 3-D effects. It may well be that this difference in optical depth is an error in the MISR retrievals due to 3-D effects or because the MISR retrieval (as do retrievals used by ISCCP and MODIS) treats all clouds as being single layer and composed of either entirely liquid or entirely ice. However, we note that other factors such as the presence of precipitation-sized particles (as well as mixed-phase particles, which are treated in ad hoc fashion by the CC retrieval) have a large impact on observed radar reflectivity and make it difficult to estimate the extinction, which is typically driven by the more numerous and smaller particles in the cloud particle size distribution. Thus, it may be that the combined CC retrieval is overestimating the optical depth or that errors in both the MISR and CC retrievals contribute significantly to the difference. At present, the exact cause of the difference in optical depths between imager-based and radar-based retrieval approaches is unclear and remains an important topic for future research beyond the scope of this article.

To be clear, the differences in the optical depth distribution are due to more than just larger optical depths for some multilayer (or vertically extensive) clouds. In particular, as discussed in the context of Figure 5, clouds which do not fill at least 50% of the CloudSat pixel (or radar resolution volume to be more accurate), according to the CALIPSO lidar, are ignored (not treated as clouds) by the combined CC retrieval. The MISR retrieval is based on 1-D radiative transfer and effectively assumes homogeneous plane parallel clouds, and one expects that these partially filled pixels will tend to have large 3-D effects in the visible and NIR radiances observed by MISR and often (though not always) result in low values for the MISR-retrieved optical depth [*Marshak et al.*, 2006; *Liang and Girolamo*, 2013].

The large occurrence in the bottom left corner of the CC-sim joint histogram is in the "no retrieval" (NR) cloud top height bin. This bin collects occurrences of columns for which the algorithm determines that the MISR retrieval would be unable to retrieve a valid cloud top height and mimics the MISR bin of the same type. All of these counts are in the $0 < \tau < 0.3$ optical depth bin in this case. In these cases, because the optical depth is so low, MISR would fail to retrieve a valid cloud top height. This is not seen in the MISR data, because clouds with such low optical depths are often not detected at all by MISR. The CC-dir histogram shows that all of these clouds are high-altitude, optically thin clouds. This also illustrates the importance of using an optical depth threshold when comparing clouds with MISR, in order to ensure that similar populations of clouds are being compared.

3.3. Regional Comparisons of Cloud Top Height and Optical Depth

In the remainder of this section, we focus on an evaluation of regional differences. Tables 1 and 2 (for January and June 2008, respectively) show low-topped, mid-topped, high-topped, and total cloud cover from MISR and CC-sim for each of the regions outlined in Figures 3 and 4. Also shown are the differences between MISR and CC-sim for each of these regions (CC-sim minus MISR retrieval), as well as the significance level of the differences calculated using a Student's *t* test (treating each orbit as an independent sample). Mid-topped and high-topped cloud amounts are in good agreement between MISR and CC-sim throughout most of the regions. The largest differences in mid-topped and high-topped cloud are in the North Pacific in January. In the North Pacific, mid-topped cloud cover is greater in CC-sim than in MISR in both months, with differences of 9.6% cloud cover in January and 5.2% cloud cover in June. The differences in high-topped cloud are larger, and differ in sign between January and June. High-topped cloud in CC-sim is less than MISR by 14.9% cloud cover in June, but is greater than MISR by 5.7% in June. These differences in the North Pacific in January may reflect biases due to incomplete wind correction in the MISR CTH-OD V6 product, and will be analyzed further in a later paper. Differences in the other regions are much smaller than this (typically less than 5% cloud cover) and are generally not statistically significant with respect to sampling.

Table 2 shows that low-topped cloud differences in June are largest in the California Stratus region, where CC-sim low-topped cloud amount (50% threshold) is lower than MISR by 12.8% cloud cover. While this region is well known for its extensive low cloud, this cloud type displays variable spatial structure and broken cloudiness. *Klein and Hartmann* [1993] find using ship-based observer reports (from the cloud atlas compiled by *Warren et al.* [1986, 1988]) that low (stratus) cloud cover in this region can exceed 60% cloud cover in summer months, reaching a peak value of 67%. This is consistent with the low-topped cloud cover found here

from MISR retrievals. *Marchand et al.* [2010] also show low-topped cloud amounts of around 60% cloud cover from ISCCP retrievals for this region (see their Figure 10). Differences between MISR and CC-sim are large in this region, but at least some of these differences may result from the diurnal cycle of stratocumulus clouds. This is explored in section 4. Low-topped cloud amounts are lower in this region in January (Table 1), and the differences are much smaller and are not statistically significant with respect to sampling.

Figure 7 shows marginal histograms of cloud top height for each of the regions outlined in Figures 3 and 4 and summarized in Tables 1 and 2 for June 2008. With the exception of the California Stratus region, the CC-dir results show large amounts of high-topped clouds. Most of this high-topped cloud is optically thin and the MISR simulator does a reasonable job matching the MISR retrievals, including capturing the altitude of the high-, mid-, and low-level cloud peaks. Low-topped differences are large in the California Stratocumulus, Hawaiian Trade Cumulus, and North Pacific regions (in the Northern Hemisphere summer) due to field-of-view issues, but these regions also have large variability in low-topped cloud amount. The differences between MISR, CC-sim, and CC-dir are qualitatively similar for January 2008 (not shown), although the magnitudes of cloud cover for each cloud top height bin are somewhat different than those shown for June 2008.

The diagnosis of cloud top height for cases involving optically thin cloud layers is notoriously challenging for passive retrievals. Retrieval of cloud top heights for such cases from MISR requires that the MISR instrument can see the cloud layer and that the stereo retrieval algorithm can identify the same cloud element in multiple camera views. Satisfying these two criteria is largely dependent on the optical thickness of the cloud layer. *Marchand et al.* [2007] compare MISR retrievals of cloud top height with cloud top heights derived from a combination of ground-based radar and lidar retrievals and categorize the height retrievals by cloud optical depth. Their analysis suggests that the MISR retrieval is generally successful in identifying the same cloud layer as the radar and lidar retrievals when the optical depth of the layer exceeds a threshold value of between 0.5 and 5.0. Based on their analysis, *Marchand and Ackerman* [2010] designed the MISR simulator to mimic this behavior, setting a default threshold of $\tau > 1.0$ for the diagnosis of optically opaque cloud layers. Because the simulated cloud top heights depend on this threshold, we examine the sensitivity of the MISR-simulated cloud top height histograms in Figure 7 to this threshold by changing the threshold value from the default of $\tau > 1$ to both $\tau > 0.5$ and $\tau > 5.0$ and reprocessing the CC retrievals of visible extinction. The results of these sensitivity tests are shown in Figure 7 with additional curves added corresponding to the $\tau > 0.5$ (dotted lines) and $\tau > 5.0$ (dashed lines) thresholds. Changing the threshold has the largest impact on the diagnosis of high-topped cloud, and as expected increasing the threshold to 5.0 results in noticeably less high-topped cloud and slightly more mid-topped cloud. In most cases the increased threshold reduces the agreement between MISR and CC-sim, suggesting that the threshold value of 1.0 is more consistent with MISR. Decreasing the threshold optical depth to 0.5 slightly increases the frequency of high-topped cloud, but the effect is much smaller and is often within the sampling uncertainty of CC-sim with the $\tau > 1.0$ threshold. These results suggest that while the MISR simulator is sensitive to the choice of thin-cloud optical depth threshold, the default value of $\tau > 1.0$ seems to provide the best agreement with MISR retrievals.

Marginal histograms of cloud optical depth from MISR and CC are shown in Figure 8 (only CC-sim is shown because the distributions for CC-sim and CC-dir are identical). The frequency of optically thin cloud ($\tau < 3.6$) is generally lower in CC than in MISR, while the frequency of optically thick cloud is generally higher in CC. These systematic differences are consistent with the earlier discussion of optical depth differences in the context of Figure 6, in which it was speculated that these differences arise due to a combination of differences in the retrievals due to 3-D effects. Figure 8 provides more insight into these differences by showing the distributions for each region. This reveals that the cloud optical depth distributions are in relatively good agreement in the North Pacific and in the California Stratocumulus regions for this month. This is consistent with these regions having more homogeneous clouds in summer months. *Di Girolamo et al.* [2010] quantify spatial heterogeneity using a combination of MISR and MODIS retrievals. They show (in Figure 1 in their manuscript) that clouds are more homogeneous (smaller heterogeneity parameter) throughout the Northern Hemisphere high latitudes and in the coastal stratocumulus regions off the coasts of California and Chile in July, and conversely are more homogeneous in Southern Hemisphere high latitudes in January. Cloud optical depth distributions for January (not shown) are in better agreement in the South Pacific, again consistent with the maps presented in *Di Girolamo et al.* [2010], lending further support to the argument that retrievals of heterogeneous clouds are driving these differences.

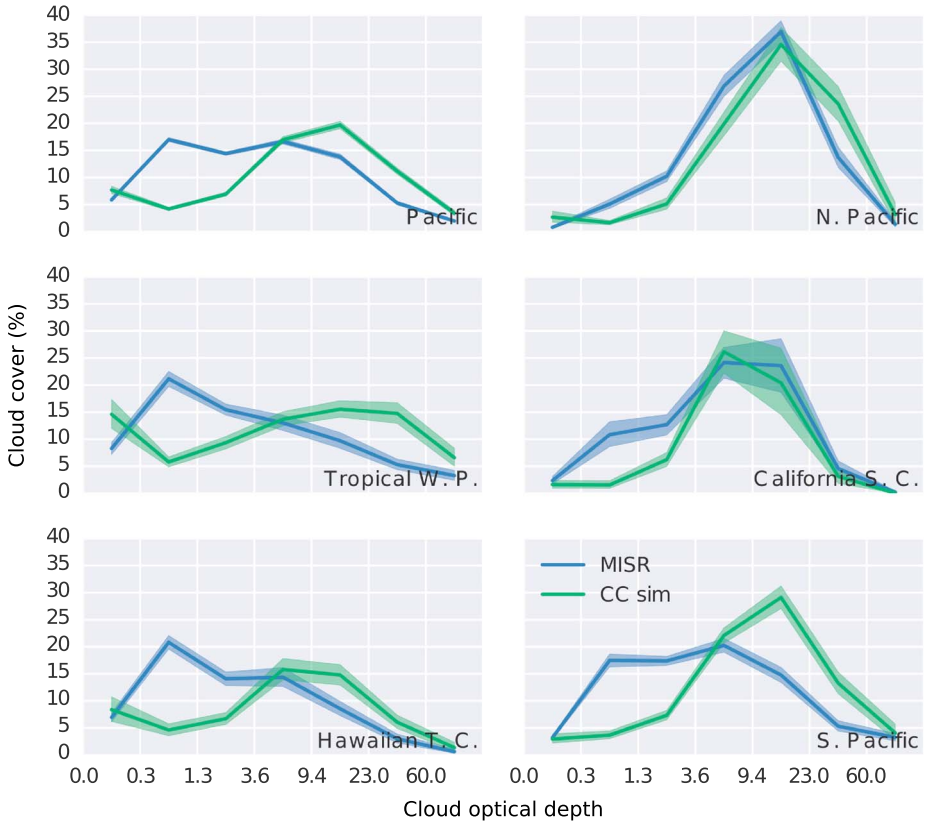

Figure 8. Marginal histograms of cloud optical depth for each of the regions defined in the text and outlined in Figure 4 for June 2008. Error bars indicate 95% confidence intervals obtained from 1000 bootstrap resamples of orbit level means.

4. Diurnal Variations in Cloud Cover

Some of the differences discussed in the previous section between MISR and CC-sim may arise due to diurnal differences in cloud height or cloud cover since MISR overpass times (on the Terra platform) are roughly 3 h different than CloudSat and CALIPSO (in the A-train constellation). There are MODIS instruments on both the Terra and Aqua (which is also in the A-train constellation) satellites, and in this section, we compare retrievals from the MODIS Terra and Aqua sensors in order to provide a measure of the differences in cloud properties between the two overpass times. Of course, some of the difference between MODIS Terra and Aqua cloud cover may be due to difference in the sensors and their performance, but these are thought to be small [*King et al.*, 2013]. *King et al.* [2013] use this strategy to evaluate diurnal differences in cloud cover by comparing 12 years of MODIS Terra (MOD35) and 9 years of Aqua (MYD35) cloud masks. They find that cloud cover over ocean is, in general, slightly greater in the Terra retrievals than in those from Aqua, suggesting a decrease in cloud cover from the morning to afternoon overpass. *King et al.* [2013] show that differences between Terra and Aqua are largest in regions dominated by coastal marine stratocumulus, and Terra to Aqua differences approach 20% cloud cover in the Peruvian and Angolan stratocumulus regions from September to February. However, zonal average differences are much smaller, and global averages agree to within 5% cloud cover between Terra and Aqua. *Meskhidze et al.* [2009] look at differences between Aqua and Terra liquid cloud amount and likewise find a reduction in both cloud amount and cloud optical depth in stratocumulus (and trade wind cumulus) regions between the morning and afternoon overpasses, with differences in the Peruvian and South African stratocumulus on the order of 20% cloud cover during the months of December to February. These results are consistent with the diurnal cycle in cloud amount expected from both modeling studies and field campaign studies, which show that cloud cover reaches a maximum in the early morning and decreases throughout the day, reaching a minimum in the early afternoon [e.g., *Bretherton et al.*, 2004].

Differences between Terra and Aqua cloud properties for the regions studied here are more modest. Differences in June-July-August total cloud cover for the California Stratus region are about 10%, and

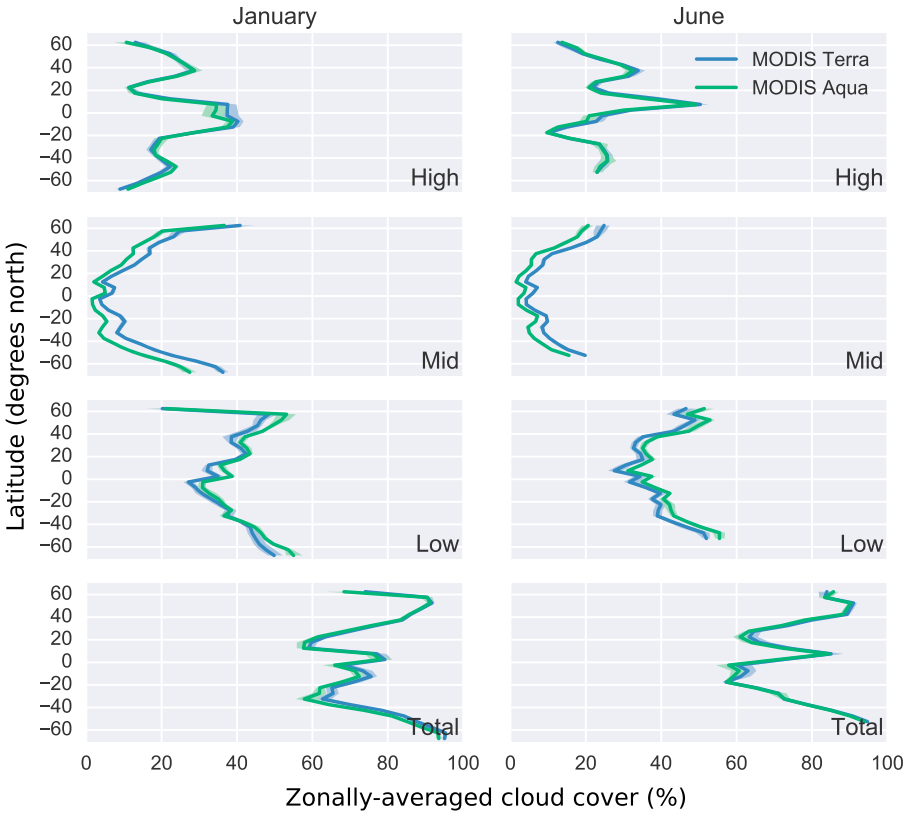

Figure 9. Zonal mean, ocean-only high-topped, mid-topped, low-topped, and total cloud cover from MODIS Terra and MODIS Aqua for (left) January and (right) June. Shaded regions indicate 95% confidence intervals with respect to sampling.

differences in the North Pacific for these months is much less than 5% [*King et al.*, 2013]. Although these differences in cloud cover are relatively small, they are of the correct sign to explain at least some of the differences between MISR and CC-sim low cloud cover shown in Table 2.

In Figure 9, we show MODIS low-topped (cloud top pressure $p_c > 680$ hPa), mid-topped ($440 < p_c < 680$ hPa), high-topped ($p_c < 440$ hPa), and total cloud cover using data from 12 years (2003 to 2014) and restricted to ocean areas in our Pacific analysis region (Figure 3). The zonal mean total cloud cover (Figure 9, bottom right) is nearly indistinguishable between the Terra and Aqua retrievals (less than 2% cloud cover difference throughout most of the domain), and the small differences that do exist in total cloud cover are not statistically significant with respect to sampling. There are, however, noticeable differences between the Terra and Aqua low-topped and mid-topped cloud cover with the Terra mid-topped cloud cover being larger than Aqua. The differences are significant in the sense that they are larger than could be explained by sampling (as represented by the error bars showing the 95% confidence interval). While these differences are modest, the differences in mid-topped and low-topped zonal mean cloud cover are slightly less than 6% and 5%, respectively. This is comparable to the difference between MISR-retrieved and MISR-simulated mid-topped cloud amount found in section 3, which suggests that this difference may be near the limit of agreement that one should expect given our evaluation approach.

In addition to diurnal differences in cloud cover, diurnal differences in cloud top height and cloud optical depth may also contribute to the differences between MISR and CC-sim shown in section 3. Figure 10 shows differences between MODIS Terra and MODIS Aqua cloud top pressure and optical depth ($p_c - \tau$) joint histograms for each of the regions studied in section 3. Differences in the distribution of cloud optical depth are small in all but the California Stratocumulus region, suggesting that diurnal differences in cloud optical depth do not contribute to the large differences in optical depth distributions from MISR and CC shown in Figure 8. The distribution of low-topped cloud optical depth is also shifted toward higher values in MODIS Terra retrievals in the California Stratocumulus region, indicating that clouds are more frequent and more

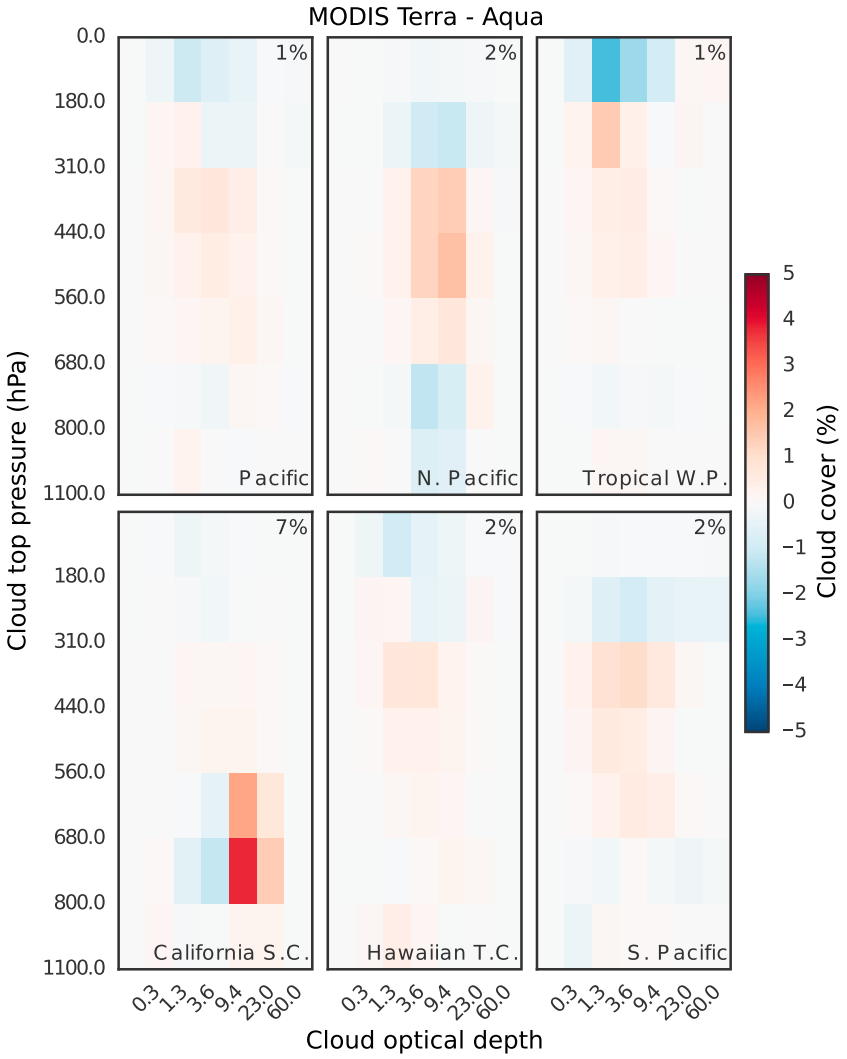

Figure 10. Differences in MODIS Terra and MODIS Aqua cloud top pressure and optical depth joint histograms for June 2008.

opaque in this region in the morning than in the afternoon. This is consistent with the known diurnal cycle of coastal stratocumulus [*Bretherton et al.*, 2004], and differences in cloud amount and optical depth in this region may be due to the fact that MISR and CC are sampling different phases in the diurnal cycle.

5. Summary and Discussion

Satellite instrument simulators are used in model evaluation studies to account for known features, limitations, or errors in individual satellite retrievals. However, not all such problems or ambiguities have been (or likely can be) removed by this approach [*Mace et al.*, 2011; *Pincus et al.*, 2012], and thus, there must be a critical evaluation of the simulators themselves. We evaluate the MISR simulator by comparing MISR retrievals to MISR-simulated retrievals based on extinction profiles derived from a combination of CloudSat, CALIPSO, MODIS, and AMSR-E observations.

The primary purpose of the MISR simulator is to specify the cloud top height that MISR would retrieve, given an input visible extinction profile. We find that mid-topped and high-topped cloud cover is in good agreement between MISR and MISR-simulated retrievals. Global, zonal, and regional averaged mid-topped and high-topped cloud cover differences are typically small (on the order of 5% cloud cover or less). Marginal histograms of cloud top height capture the main features of the cloud top height distribution, including the altitude of peaks in cloud top height. The most notable exception to this is high-topped cloud amounts in the

winter hemisphere poleward of 50°, where differences are closer to 10%. It is expected that this problem will be reduced in the next release (Version 7) of the MISR CTH-OD data set, which we expect to analyze when it becomes available.

Uncertainties in low-topped cloud remain large in this comparison. Differences between MISR and CC-sim are between 5 and 15% cloud cover for the specific regions studied here, and differences in MISR and CC-sim zonal means often exceed 10% cloud cover. This is likely due to partially filled cloudy pixels rather than being indicative of a problem with the MISR simulator.

Differences in the full cloud top height and optical depth joint histograms for the whole domain have an absolute error of 4% or less for any particular cloud type ($z_c - \tau$ bin). This is similar to results from M2011, who considered coincident ISCCP and ISCCP-simulated retrievals derived from ARM SGP data and report absolute errors in the coarsened nine-bin ISCCP histograms that are typically under 4% as well, but can be as high as 8% for low, optically thick clouds (see Figure 4 in M2011). Much of the difference in the observed MISR (or ISCCP) histogram and that obtained from the simulator (using CC retrievals as input) is due to a systematic trend toward higher values of cloud optical depth in the CC retrieval than in MISR (or ISCCP) retrievals. For low clouds, the effect of sensor resolution and 3-D effects on visible radiances may explain much or most of the difference. The situation is less clear for high-level and midlevel clouds, which tend to occur on larger horizontal scales. While 3-D effects may still be significant for high-level and midlevel clouds, other factors may also be important. In particular, retrievals of optical depth from radar and lidar may be prone to overestimate optical depth for a variety of factors including the strong sensitivity of radar to precipitating particles (which makes retrieval of small or nonprecipitating particles that usually dominate the visible extinction difficult and uncertain), especially at temperatures where both ice and water condensate may exists.

The optical depth retrieval uncertainties (which are not corrected for in the MISR or ISCCP simulators) make interpretation of differences between retrieved and modeled optical depth distributions difficult, especially when combined into a joint histogram with cloud top height. Nonetheless, the MISR simulator is a useful tool for model evaluation as is. Many climate models are beginning to incorporate so-called PDF schemes to represent boundary layer variability, and in the future, we speculate that it may well be possible to extend these schemes to represent (or parameterize) cloud condensate variability and account for some of the optical depth difficulties in the simulator.

Acknowledgments

Funding for this research was provided by the MISR project at the NASA Jet Propulsion Laboratory (under contract 1318945). B.R.H., R.T.M., and T.P.A. also were supported in part by funding from the Center for Multiscale Modeling of Atmospheric Processes (NSF Science and Technology Center) at Colorado State University under subaward ATM-0425247 to the University of Washington. G.M. and S.B. provided the CloudSat/CALIPSO visible extinction retrieval, funded by NASA grant NNX13AQ34G. B.R.H., R.T.M., and T.P.A. are grateful to David Diner, Principal Investigator of the MISR instrument, for his continual interest in and support of this research. We also acknowledge the many contributions of the MISR instrument team at JPL that enabled our research and made this project possible. MISR orbit level data and CloudSat/CALIPSO visible extinction retrievals used here are available by special request to the corresponding author (bhillma@sandia.gov).

References

Ackerman, T. P., and G. M. Stokes (2003), The atmospheric radiation measurement program, *Phys. Today*, *56*, 38–44.

Berry, E., and G. G. Mace (2014), Cloud properties and radiative effects of the Asian summer monsoon derived from A-train data, *J. Geophys. Res. Atmos.*, *119*, 9492–9508, doi:10.1002/2014JD021458.

Bony, S., and J.-L. Dufresne (2005), Marine boundary layer clouds at the heart of tropical cloud feedback uncertainties in climate models, *Geophys. Res. Lett.*, *32*, L20806, doi:10.1029/2005GL023851.

Bony, S., et al. (2006), How well do we understand and evaluate climate change feedback processes?, *J. Clim.*, *19*(15), 3445–3482, doi:10.1175/JCLI3819.1.

Bretherton, C. S., T. Uttal, C. W. Fairall, S. E. Yuter, R. A. Weller, D. Baumgardner, K. Comstock, R. Wood, and G. B. Raga (2004), The EPIC 2001 stratocumulus study, *Bull. Am. Meteorol. Soc.*, *85*(7), 967–977, doi:10.1175/BAMS-85-7-967.

Cess, R. D., et al. (1990), Intercomparison and interpretation of climate feedback processes in 19 atmospheric general circulation models, *J. Geophys. Res.*, *95*(D10), 16,601–16,615, doi:10.1029/JD095iD10p16601.

Deng, M., G. G. Mace, Z. Wang, and H. Okamoto (2010), Tropical composition, cloud and climate coupling experiment validation for cirrus cloud profiling retrieval using CloudSat radar and CALIPSO lidar, *J. Geophys. Res.*, *115*, D00J15, doi:10.1029/2009JD013104.

Deng, M., G. G. Mace, Z. Wang, and R. P. Lawson (2013), Evaluation of several A-train ice cloud retrieval products with in situ measurements collected during the SPARTICUS campaign, *J. Appl. Meteorol. Climatol.*, *52*(4), 1014–1030.

Dey, S., L. Di Girolamo, and G. Zhao (2008), Scale effect on statistics of the macrophysical properties of trade wind cumuli over the tropical western Atlantic during RICO, *J. Geophys. Res.*, *113*, D24214, doi:10.1029/2008JD010295.

Di Girolamo, L., and R. Davies (1997), Cloud fraction errors caused by finite resolution measurements, *J. Geophys. Res.*, *102*(D2), 1739–1756, doi:10.1029/96JD02663.

Di Girolamo, L., L. Liang, and S. Platnick (2010), A global view of one-dimensional solar radiative transfer through oceanic water clouds, *Geophys. Res. Lett.*, *37*, L18809, doi:10.1029/2010GL044094.

Diner, D. J., J. C. Beckert, G. W. Bothwell, and J. I. Rodriguez (2002), Performance of the MISR instrument during its first 20 months in Earth orbit, *IEEE Trans. Geosci. Remote Sens.*, *40*(7), 1449–1466, doi:10.1109/TGRS.2002.801584.

Diner, D. J., et al. (2005), The value of multiangle measurements for retrieving structurally and radiatively consistent properties of clouds, aerosols, and surfaces, *Remote Sens. Environ.*, *97*(4), 495–518, doi:10.1016/j.rse.2005.06.006.

Dong, X., and G. G. Mace (2003), Profiles of low-level stratus cloud microphysics deduced from ground-based measurements, *J. Atmos. Oceanic Technol.*, *20*(1), 42–53.

Dufresne, J.-L., and S. Bony (2008), An assessment of the primary sources of spread of global warming estimates from coupled atmosphere-ocean models, *J. Clim.*, *21*, 5135–5144, doi:10.1175/2008JCLI2239.1.

Efron, B., and R. J. Tibshirani (1994), *An Introduction to the Bootstrap*, CRC Press, New York.

Jones, A. L., L. Di Girolamo, and G. Zhao (2012), Reducing the resolution bias in cloud fraction from satellite derived clear-conservative cloud masks, *J. Geophys. Res.*, *117*, D12201, doi:10.1029/2011JD017195.
Kay, J. E., et al. (2012), Exposing global cloud biases in the Community Atmosphere Model (CAM) using satellite observations and their corresponding instrument simulators, *J. Clim.*, *25*, 5190–5207, doi:10.1175/JCLI-D-11-00469.1.
King, M. D., W. P. Menzel, Y. J. Kaufman, D. Tanré, B.-C. Gao, S. Platnick, S. A. Ackerman, L. A. Remer, R. Pincus, and P. A. Hubanks (2003), Cloud and aerosol properties, precipitable water, and profiles of temperature and water vapor from MODIS, *IEEE Trans. Geosci. Remote Sens.*, *41*(2), 442–458, doi:10.1109/TGRS.2002.808226.
King, M. D., S. Platnick, W. P. Menzel, S. A. Ackerman, and P. A. Hubanks (2013), Spatial and temporal distribution of clouds observed by MODIS onboard the Terra and Aqua satellites, *IEEE Trans. Geosci. Remote Sens.*, *51*(7), 3826–3852, doi:10.1109/TGRS.2012.2227333.
Klein, S. A., and D. L. Hartmann (1993), The seasonal cycle of low stratiform clouds, *J. Clim.*, *6*(8), 1587–1606, doi:10.1175/1520-0442(1993)006<1587:TSCOLS>2.0.CO;2.
Klein, S. A., and C. Jakob (1999), Validation and sensitivities of frontal clouds simulated by the ECMWF model, *Mon. Weather Rev.*, *127*(10), 2514–2531, doi:10.1175/1520-0493(1999)127<2514:VASOFC>2.0.CO;2.
Klein, S. A., Y. Zhang, M. D. Zelinka, R. Pincus, J. Boyle, and P. J. Gleckler (2013), Are climate model simulations of clouds improving? An evaluation using the ISCCP simulator, *J. Geophys. Res. Atmos.*, *118*, 1329–1342, doi:10.1002/jgrd.50141.
Liang, L., and L. D. Girolamo (2013), A global analysis on the view-angle dependence of plane-parallel oceanic liquid water cloud optical thickness using data synergy from MISR and MODIS, *J. Geophys. Res. Atmos.*, *118*, 2389–2403, doi:10.1029/2012JD018201.
Lin, W. Y., and M. H. Zhang (2004), Evaluation of clouds and their radiative effects simulated by the NCAR Community Atmospheric Model against satellite observations, *J. Clim.*, *17*(17), 3302–3318, doi:10.1175/1520-0442(2004)017<3302:EOCATR>2.0.CO;2.
Mace, G. G. (2010), Cloud properties and radiative forcing over the maritime storm tracks of the Southern Ocean and North Atlantic derived from A-train, *J. Geophys. Res.*, *115*, D10201, doi:10.1029/2009JD012517.
Mace, G. G., and F. J. Wrenn (2013), Evaluation of the hydrometeor layers in the East and West Pacific within ISCCP cloud-top pressure-optical depth bins using merged CloudSat and CALIPSO data, *J. Clim.*, *26*, 9429–9444, doi:10.1175/JCLI-D-12-00207.1.
Mace, G. G., and Q. Zhang (2014), The CloudSat radar-lidar geometrical profile product (RL-GeoProf): Updates, improvements, and selected results, *J. Geophys. Res. Atmos.*, *119*, 9441–9462, doi:10.1002/2013JD021374.
Mace, G. G., et al. (2006), Cloud radiative forcing at the atmospheric radiation measurement program climate research facility: 1. Technique, validation, and comparison to satellite-derived diagnostic quantities, *J. Geophys. Res.*, *111*, D11S90, doi:10.1029/2005JD005921.
Mace, G. G., Q. Zhang, M. Vaughan, R. Marchand, G. Stephens, C. Trepte, and D. Winker (2009), A description of hydrometeor layer occurrence statistics derived from the first year of merged Cloudsat and CALIPSO data, *J. Geophys. Res.*, *114*, DO0A26, doi:10.1029/2007JD009755.
Mace, G. G., S. Houser, S. Benson, S. A. Klein, and Q. Min (2011), Critical evaluation of the ISCCP simulator using ground-based remote sensing data, *J. Clim.*, *24*(6), 1598–1612, doi:10.1175/2010JCLI3517.1.
Marchand, R., and T. Ackerman (2010), An analysis of cloud cover in multiscale modeling framework global climate model simulations using 4 and 1 km horizontal grids, *J. Geophys. Res.*, *115*, D16207, doi:10.1029/2009JD013423.
Marchand, R., T. Ackerman, M. Smyth, and W. B. Rossow (2010), A review of cloud top height and optical depth histograms from MISR, ISCCP and MODIS, *J. Geophys. Res.*, *115*, D16206, doi:10.1029/2009JD013422.
Marchand, R. T., T. P. Ackerman, M. D. King, C. Moroney, R. Davies, J.-P. Muller, and H. Gerber (2001), Multiangle observations of Arctic clouds from FIRE ACE: June 3, 1998, case study, *J. Geophys. Res.*, *106*(D14), 15–201.
Marchand, R. T., T. P. Ackerman, and C. Moroney (2007), An assessment of Multiangle Imaging Spectroradiometer (MISR) stereo-derived cloud top heights and cloud top winds using ground-based radar, lidar, and microwave radiometers, *J. Geophys. Res.*, *112*, D06204, doi:10.1029/2006JD007091.
Marshak, A., S. Platnick, T. Várnai, G. Wen, and R. F. Cahalan (2006), Impact of three-dimensional radiative effects on satellite retrievals of cloud droplet sizes, *J. Geophys. Res.*, *111*, D09207, doi:10.1029/2005JD006686.
Medeiros, B., B. Stevens, I. M. Held, M. Zhao, D. L. Williamson, J. G. Olson, and C. S. Bretherton (2008), Aquaplanets, climate sensitivity, and low clouds, *J. Clim.*, *21*(19), 4974–4991, doi:10.1175/2008JCLI1995.1.
Meskhidze, N., L. Remer, S. Platnick, R. N. Juárez, A. Lichtenberger, and A. Aiyyer (2009), Exploring the differences in cloud properties observed by the Terra and Aqua MODIS sensors, *Atmos. Chem. Phys. Discuss.*, *9*(10), 3461–3475.
Moroney, C., R. Davies, and J.-P. Muller (2002), Operational retrieval of cloud-top heights using MISR data, *IEEE Trans. Geosci. Remote Sens.*, *40*(7), 1532–1540, doi:10.1109/TGRS.2002.801150.
Muller, J.-P., A. Mandanayake, C. Moroney, R. Davies, D. J. Diner, and S. Paradise (2002), MISR stereoscopic image matchers: Techniques and results, *IEEE Trans. Geosci. Remote Sens.*, *40*(7), 1547–1559, doi:10.1109/TGRS.2002.801160.
Naud, C., J.-P. Muller, and E. E. Clothiaux (2002), Comparison of cloud top heights derived from MISR stereo and MODIS CO_2-slicing, *Geophys. Res. Lett.*, *29*(16), 1795, doi:10.1029/2002GL015460.
Naud, C., J.-P. Muller, M. Haeffelin, Y. Morille, and A. Delaval (2004), Assessment of MISR and MODIS cloud top heights through inter-comparison with a back-scattering lidar at SIRTA, *Geophys. Res. Lett.*, *31*, L04114, doi:10.1029/2003GL018976.
Naud, C., J.-P. Muller, E. Clothiaux, B. Baum, and W. Menzel (2005), Intercomparison of multiple years of MODIS, MISR and radar cloud-top heights, *Ann. Geophys.*, *23*, 2415–2424. Copernicus GmbH.
Norris, J. R., and C. P. Weaver (2001), Improved techniques for evaluating GCM cloudiness applied to the NCAR CCM3, *J. Clim.*, *14*(12), 2540–2550, doi:10.1175/1520-0442(2001)014<2540:ITFEGC>2.0.CO;2.
Pincus, R., S. Platnick, S. A. Ackerman, R. S. Hemler, and R. J. P. Hofmann (2012), Reconciling simulated and observed views of clouds: MODIS, ISCCP, and the limits of instrument simulators, *J. Clim.*, *25*, 4699–4720, doi:10.1175/JCLI-D-11-00267.1.
Rossow, W. B., and R. A. Schiffer (1999), Advances in understanding clouds from ISCCP, *Bull. Am. Meteorol. Soc.*, *80*(11), 2261–2287, doi:10.1175/1520-0477(1999)080<2261:AIUCFI>2.0.CO;2.
Seiz, G., R. Davies, and A. Grün (2006), Stereo cloud-top height retrieval with ASTER and MISR, *Int. J. Remote Sens.*, *27*(9), 1839–1853.
Warren, S. G., C. J. Hahn, J. London, R. M. Chervin, and R. L. Jenne, (1986), Global distribution of total cloud cover and cloud type amounts over land, Tech. Rep., Washington Univ., Dept. of Atmos. Sci., Colorado Univ., Natl. Cent. for Atmos. Res., Seattle, and Boulder, Colo.
Warren, S. G., C. J. Hahn, J. London, R. M. Chervin, and R. L. Jenne, (1988), Global distribution of total cloud cover and cloud type amounts over the ocean, *Tech. Rep.*, US-DOE Off. of Energy Res., Carbon Dioxide Res. Div., Natl. Cen. for Atmos. Res., Washington, D. C., Boulder, Colo.
Webb, M., C. Senior, S. Bony, and J.-J. Morcrette (2001), Combining ERBE and ISCCP data to assess clouds in the Hadley Centre, ECMWF and LMD atmospheric climate models, *Clim. Dyn.*, *17*(12), 905–922, doi:10.1007/s003820100157.
Wielicki, B. A., and L. Parker (1992), On the determination of cloud cover from satellite sensors: The effect of sensor spatial resolution, *J. Geophys. Res.*, *97*(D12), 12,799–12,823, doi:10.1029/92JD01061.

Wilks, D. S. (2011), *Statistical Methods in the Atmospheric Sciences*, vol. 100, Academic Press, Waltham, Mass.

Williams, K. D., and M. J. Webb (2009), A quantitative performance assessment of cloud regimes in climate models, *Clim. Dyn.*, *33*(1), 141–157, doi:10.1007/s00382-008-0443-1.

Wyant, M. C., C. S. Bretherton, J. T. Bacmeister, J. T. Kiehl, I. M. Held, M. Zhao, S. A. Klein, and B. J. Soden (2006), A comparison of low-latitude cloud properties and their response to climate change in three AGCMs sorted into regimes using mid-tropospheric vertical velocity, *Clim. Dyn.*, *27*(2–3), 261–279.

Zhang, M., et al. (2005), Comparing clouds and their seasonal variations in 10 atmospheric general circulation models with satellite measurements, *J. Geophys. Res.*, *110*, D15S02, doi:10.1029/2004JD005021.

Zhao, G., and L. Di Girolamo (2006), Cloud fraction errors for trade wind cumuli from EOS-Terra instruments, *Geophys. Res. Lett.*, *33*, L20802, doi:10.1029/2006GL027088.